

## Article

# Investigating Crude Sesame Oil Sedimentation and Its Monitoring Using Laser Backscattering Imaging (LBI)

Zhangkai Wu <sup>1,\*</sup> , Sebastian Romuli <sup>1</sup> , Kiatkamjon Intani <sup>1,2</sup>  and Joachim Müller <sup>1</sup> 

<sup>1</sup> Tropics and Subtropics Group (440e), Institute of Agricultural Engineering, University of Hohenheim, 70599 Stuttgart, Germany; sebastian\_romuli@uni-hohenheim.de (S.R.); kiatkamjon.i@ku.th (K.I.); joachim.mueller@uni-hohenheim.de (J.M.)

<sup>2</sup> Department of Farm Mechanics, Faculty of Agriculture, Kasetsart University, Bangkok 10900, Thailand

\* Correspondence: info440e@uni-hohenheim.de; Tel.: +49-(0)711-459-22840; Fax: +49-(0)711-459-23298

**Abstract:** Sesame oil is a food and energy resource that is not used enough. Sedimentation of crude oil after pressing can remove particles and happens regardless of the producer's intention. However, sedimentation of crude plant oil and its sensing technology are rarely studied. This research studied crude sesame oil sedimentation and monitored it with low-cost laser backscattering imaging (LBI). In the discontinuous measurement, a 30-day sedimentation was conducted with oil samples sent to the lab LBI system for image capture. A scattering spot and an increasing Tyndall effect along the light path were seen. In the continuous measurement, an LBI system was mounted on a sedimentation tank for 30 days. The sedimentation curve, scattering images, and oil properties were checked. The sedimentation speed was about  $-7$  mm/h, then less than  $-2$  mm/h. The image features correlated well with the sedimentation interface height ( $R^2 = 0.97$ ) when the height was above  $-100$  mm. The oil-particle-related properties (ash content, phosphorus content, carbon residue, and total contamination) dropped by at least 87%, water content decreased by 90%, and the oxidation-related properties (oxidation stability,  $\gamma$ -tocotrienol,  $\delta$ -tocopherol,  $\gamma$ -tocopherol, and acid value) changed less significantly. The crude sesame oil sedimentation had two stages: diluted and hindered sedimentation. This research can help improve sedimentation tank and LBI system design and prevent unwanted sedimentation.

**Keywords:** batch settling curve; laser backscattering imaging; rancidification; *Sesamum indicum* L.; settling tank; turbidity



**Citation:** Wu, Z.; Romuli, S.; Intani, K.; Müller, J. Investigating Crude Sesame Oil Sedimentation and Its Monitoring Using Laser Backscattering Imaging (LBI). *Appl. Sci.* **2023**, *13*, 9013. <https://doi.org/10.3390/app13159013>

Academic Editor: Alessio Tugnolo

Received: 7 July 2023

Revised: 3 August 2023

Accepted: 5 August 2023

Published: 7 August 2023



**Copyright:** © 2023 by the authors. Licensee MDPI, Basel, Switzerland. This article is an open access article distributed under the terms and conditions of the Creative Commons Attribution (CC BY) license (<https://creativecommons.org/licenses/by/4.0/>).

## 1. Introduction

In 2020, global sesame oil production was 1 million metric tons, with Sudan being the leading producer of sesame seeds [1]. Sesame oil is widely known for its use in the cosmetic industry, cooking, and medicine [2–4]. Langyan et al. suggested that the nutritional and health benefits of sesame oil are not fully utilized [5]. Furthermore, due to the growing demand for renewable energy, researchers are considering using sesame oil as a source of biodiesel [6–8].

Gravity separation, also known as sedimentation [9], is a simple method for removing solid impurities from crude plant oil [10,11]. It is a physical process where suspended solid particles in a liquid undergo gravitational settling and accumulate at the bottom of the container, resulting in a clearer supernatant. Sedimentation for crude oil purification is not commonly used in the industry due to its low efficiency, while the filtration process is prevalent [10,12]. However, Altieri et al. suggested that applying an assisted sedimentation system could save energy and improve olive oil quality on an industrial scale [13]. Additionally, sedimentation is a suitable method to reduce total contamination in plant oil for energy use in rural areas [14,15]. Short-term oil sedimentation could be used as a pre-processing step before filtering [16]. In the last decade, the technology for

designing sedimentation tanks has developed a lot in the field of treating wastewater [17], which has the potential to also benefit the design of oil sedimentation tanks. Notably, once plant oils are pressed and stored in a container, sedimentation occurs regardless of the producer's intention. For instance, sediment in unrefined oil products requires additional explanation from sellers to reassure consumers [18]. The fundamental theory of sedimentation in physics indicates that the sedimentation process might encompass several distinct stages. These stages include diluted sedimentation, which is characterized by a constant sedimentation speed, and hindered sedimentation, distinguished by the evolution of a distinct supernatant–sediment interface [19]. However, the sedimentation process could vary depending on practical situations. For example, Pietsch et al. found that no diluted sedimentation occurred in a biogas fermenter due to the fibrous structure of the substrate particles [20]. Few studies have been conducted to investigate the sedimentation stages of plant oil; therefore, further research is needed to help maximize the potential use and minimize the drawbacks.

Laser backscattering imaging (LBI) is a non-destructive optical technique that exploits the scattering effect of porous objects when illuminated by a laser beam. The resulting scattering pattern images are analyzed to extract object information. LBI exhibits potential in numerous agricultural domains [21–23]. Since the concentration of suspended solid particles in sedimentation fluctuates, LBI may have the potential to monitor the oil sedimentation process. Additionally, the affordability and non-invasive nature of LBI make it particularly suitable for application in rural areas or small-scale factories. Thus, the objective of this study was to investigate the crude sesame oil sedimentation process with an LBI system.

## 2. Materials and Methods

### 2.1. Sesame Oil

Sesame seeds (Sesame S42 White) were imported from Bobo-Dioulasso (Burkina Faso). The seeds, with an initial moisture content of 3%, were re-moistened to 8% at 10 kg per unit, by adding distilled water as described in [24]. Sesame oil was mechanically extracted by pressing the seeds with a spindle press (KK20 F Universal, Kern Kraft oil press GmbH & Co. KG, Reut, Germany) and stored in 10 L containers.

### 2.2. Experimental Setup for Discontinuous LBI Measurement

A discontinuous LBI measurement experiment was conducted to investigate the interaction between the laser and sesame oil during the sedimentation process. The sedimentation lasted for 30 days, with the room temperature ranging from 20 to 25 °C. Twenty-nine liters of crude sesame oil, stored at a temperature below 5 °C, was warmed up under room temperature for 24 h and then poured into a 30 L open container. The container was left open to promote oxidation of the oil. A stirrer was used to homogenize the oil. At Day 0, Day 5, Day 20, and Day 30, oil samples were taken out from the top of the sedimentation tank and filled in transparent plastic cylindrical bottles (34 mm diameter, 69 mm height) at a height of 66 mm for the LBI system to capture images. The LBI system in a black box, as illustrated in Figure 1, consisted of two lasers with wavelengths of 635 nm (LFD635-1-3, Picotronic, Koblenz, Germany) and 405 nm (DD405-1-3, Picotronic, Koblenz, Germany), and a camera (PX5-CM, PAX cam, Villa Park, IL, USA) equipped with a zoom lens. The size of the images was 2592 × 1944 pixels. The distance between the camera lens and the surface of the oil sample was 190 mm, enlarging the scattering phenomenon while ensuring that the image boundary was not exceeded. To ensure stable laser light during measurement, the laser was turned on for a minimum of 15 min before image capture.

### 2.3. Experimental Setup for Continuous LBI Measurement

In addition, an LBI system was directly mounted on a sedimentation tank to perform continuous LBI measurements during the sedimentation process (Figure 2). The sedimentation process lasted for 30 days; during the experiment, the oil temperature was  $21 \pm 3$  °C.

About 120 L of pressed crude oil was homogenized and poured into a transparent acrylic glass cylindrical tank (500 mm diameter, 1000 mm height), with a transparent acrylic glass lid put on the top. The crude oil height in the tank was 592 mm. The LBI system mounted on top of the tank consisted of a red laser (DC650-1-3-HT-CON-JST, Picotronic, Koblenz, Germany) and camera 1 (ELP-USBFHD01M-BFV, Ailipu, Shenzhen, China). To minimize the direct laser light reflection and at the same time optimize the laser light penetration into the sesame oil, the incident angles of the lasers were set at  $15^\circ$  to vertical direction [21]. The image taken by camera 1 had a size of  $1920 \times 1080$  pixels with a resolution of 0.3 mm/pixel. A one-meter rule was pasted onto the oil tank, and camera 2 and camera 3 (same type as camera 1) were mounted at side positions to observe the interface between sediment and supernatant. All three cameras and lights were connected to a computer. As cameras 2 and 3 could not capture the complete view of the tank, manual images were taken from a larger distance every 24 h. Images were automatically taken every hour by camera 2 and camera 3 to measure the sediment's height. Afterwards, the light was automatically turned off for camera 1 to take an LBI image. When the oil interface height changed by 1 mm or more, the corresponding time was recorded. Both the time and interface height were used for further data analysis.

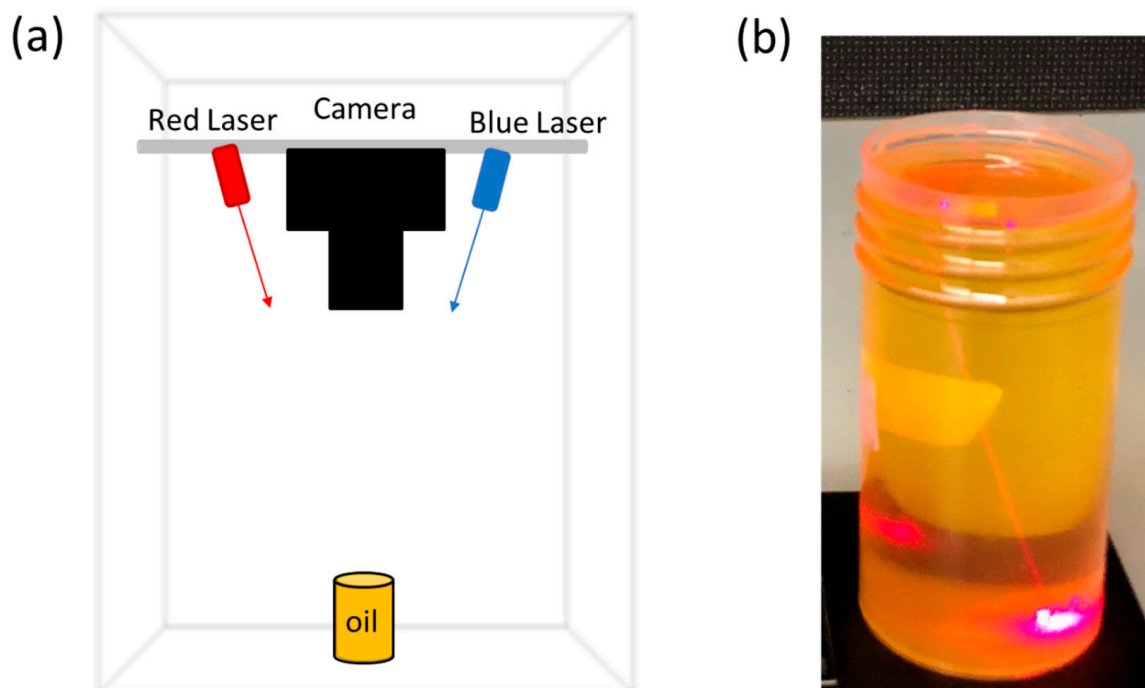


**Figure 1.** (a) The imaging system setup employed for discontinuous LBI (laser backscattering imaging) measurement; (b) the experimental phenomena with clean sesame oil when subjected to red laser illumination.

#### 2.4. Image Analysis

For the analysis of the LBI images in the continuous experiment, an  $80 \times 80$  pixel box at a fixed position in the image was used to segment the backscattering area from the background (Figure 2) followed by a  $3 \times 3$  median filter to reduce the noise in the images. The mean grey value of the segmented image was used as the feature of the LBI images:

$$I_{mean} = \frac{I_R + I_G + I_B}{3} \times \frac{1}{80 \times 80} \quad (1)$$

where  $I_R$ ,  $I_G$ ,  $I_B$  are the red, green, and blue channel intensity, respectively, on a scale of 0–255.

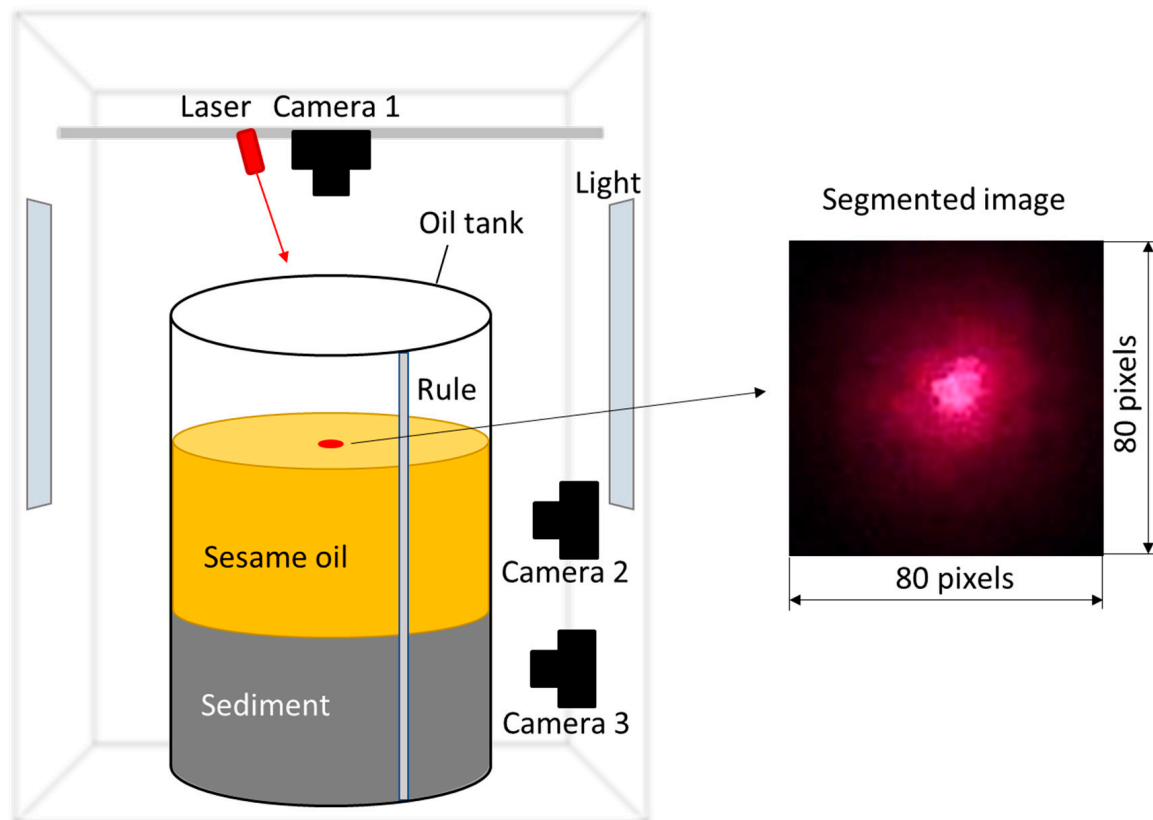


**Figure 2.** The system setup used for continuous LBI measurements, with an example image captured by camera 1 and segmented by an  $80 \times 80$  pixel box.

### 2.5. Chemical Analysis

At the beginning and end of the continuous LBI measurement, the following chemical properties were measured (Table 1): ash content, phosphorus content, carbon residue, total contamination, water content, oxidation stability, vitamin E ( $\gamma$ -tocotrienol,  $\delta$ -tocopherol and  $\gamma$ -tocopherol), and acid value.

**Table 1.** Measurement methods used for continuous LBI measurement.

Oil Parameter	Unit	Method or Instrument
Ash content	% (m/m)	ISO 6884 [25]
Phosphorus content	mg/kg	DIN EN ISO 11885 <sup>1</sup> [26] DIN EN 14107 [27]
Carbon residue	% (m/m)	DIN EN ISO 10370 [28]
Total contamination	mg/kg	DIN EN 12662 [29]
Water content	% (m/m)	DIN 12937 [30]
Oxidation stability	h	DIN EN 14112 [31]
$\gamma$ -Tocotrienol	$\mu\text{g/g}$	Grebenstein and Frank, 2012 [32]
$\delta$ -Tocopherol	$\mu\text{g/g}$	Grebenstein and Frank, 2012 [32]
$\gamma$ -Tocopherol	$\mu\text{g/g}$	Grebenstein and Frank, 2012 [32]
Acid value	mg KOH/g	SI Analytics [33]

<sup>1</sup> Performed after microwave digestion due to the high presence of particles in the crude oil.

### 2.6. Statistical Analysis

The statistical analysis in this research was performed with OriginPro (Version 2020, OriginLab, Northampton, MA, USA). R squared ( $R^2$ ) was used as the indicator of goodness of fit. To smoothen the plot of sedimentation velocity vs. time, a moving average function was applied with the period parameter set to 8.

### 3. Results and Discussion

#### 3.1. Discontinuous LBI Measurement

Figure 3 shows the backscattering images of oil samples from discontinuous LBI measurement. At Day 0, the crude oil displayed a typical backscattering pattern on the sample surface. Gradually, the laser images showed a linear shape with increasing length over time, indicating the path of the laser light (Tyndall effect). The intensity of the linear pattern decreased in the direction of light transmission. For the red laser, an additional scattering pattern was observed on the right side of the image due to excessive light reaching the bottom of the sample container. Notably, yellow hues were visible between the overexposed center and the surrounding scattering area for the red laser, and purple hues for the blue laser.

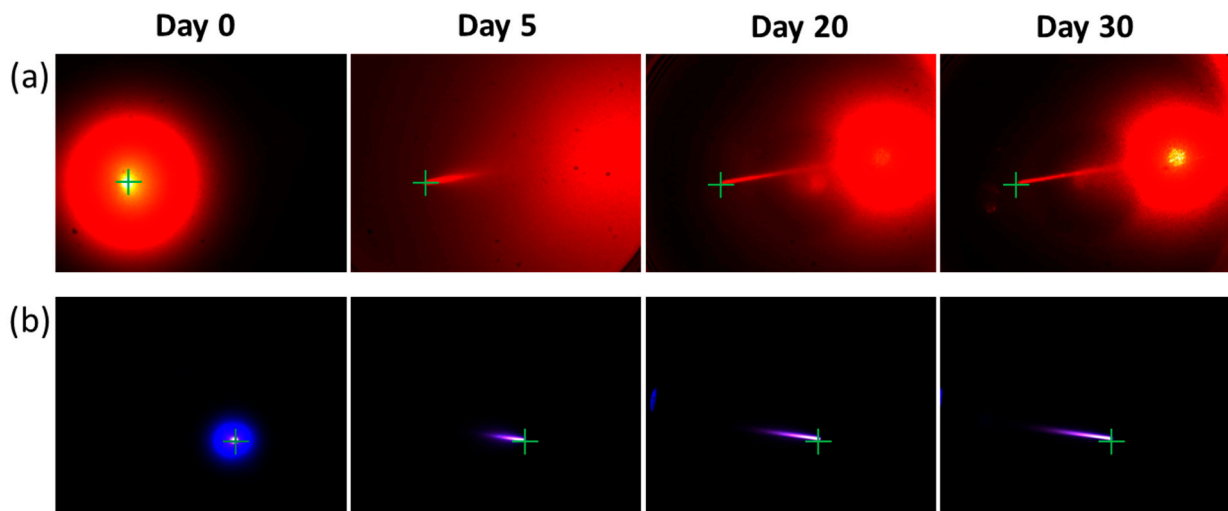


**Figure 3.** Backscattering images of oil samples under (a) the 635 nm laser and (b) the 405 nm laser. The crosses in the images indicate the incident points where the laser light entered the surface of the oil. Note that the light from the 635 nm laser transmitted from left to right, reaching the bottom of the container as the oil became clearer. The 405 nm laser transmitted light from right to left.

At Day 0 of sedimentation, the round scattering spot can be attributed to the laser light interacting with particles that were still uniformly dispersed in the crude oil. Similar scattering spots were observed by other scientists when handling bio-materials [34–36] due to the porous nature of bio-materials. Wu et al. suggested that this scattering spot should be related to the particle size of the material [37]. As the oil became clearer, laser light could travel deeper because there were fewer particles present to scatter and absorb the light, causing the scattering spot at the incident point to shrink. The Tyndall effect suggests that some particles remained within the oil even after sedimentation, which aligns with the research findings by Karaj and Müller [15]. They found that the sedimentation process predominantly impacts particles of substantial size. Huang et al. applied the Tyndall effect to detect  $\text{Hg}^{2+}$  in a colloidal solution and found that this method increased accuracy by 5400 times compared to the traditional approach [38].

#### 3.2. Continuous LBI Measurement

##### 3.2.1. Sesame Oil Sedimentation Dynamics

During the sedimentation process of crude sesame oil, the oil and the sediment were divided, with an increasingly distinct interface (Figure 4). After 720 h of sedimentation, 493 mm of clear oil was obtained from the initial height of the crude oil layer of 592 mm. The change in interface height and sedimentation velocity over time are illustrated in Figure 5. The sedimentation velocity remained close to  $-7$  mm/h until about 25 h of the sedimentation. Afterwards, the velocity decreased to  $-2$  mm/h within about 15 h, then

gradually dropped to a value close to 0. Linear and exponential regressions were performed to fit the curves within 0–39 h and 39–720 h, respectively. The timepoint 39 h was fitted as the turning point, since the  $R^2$  of the linear regression remained above 0.999 between 0 and 39 h and dropped below 0.999 after 40 h. Both regressions showed an  $R^2$  value close to 1.

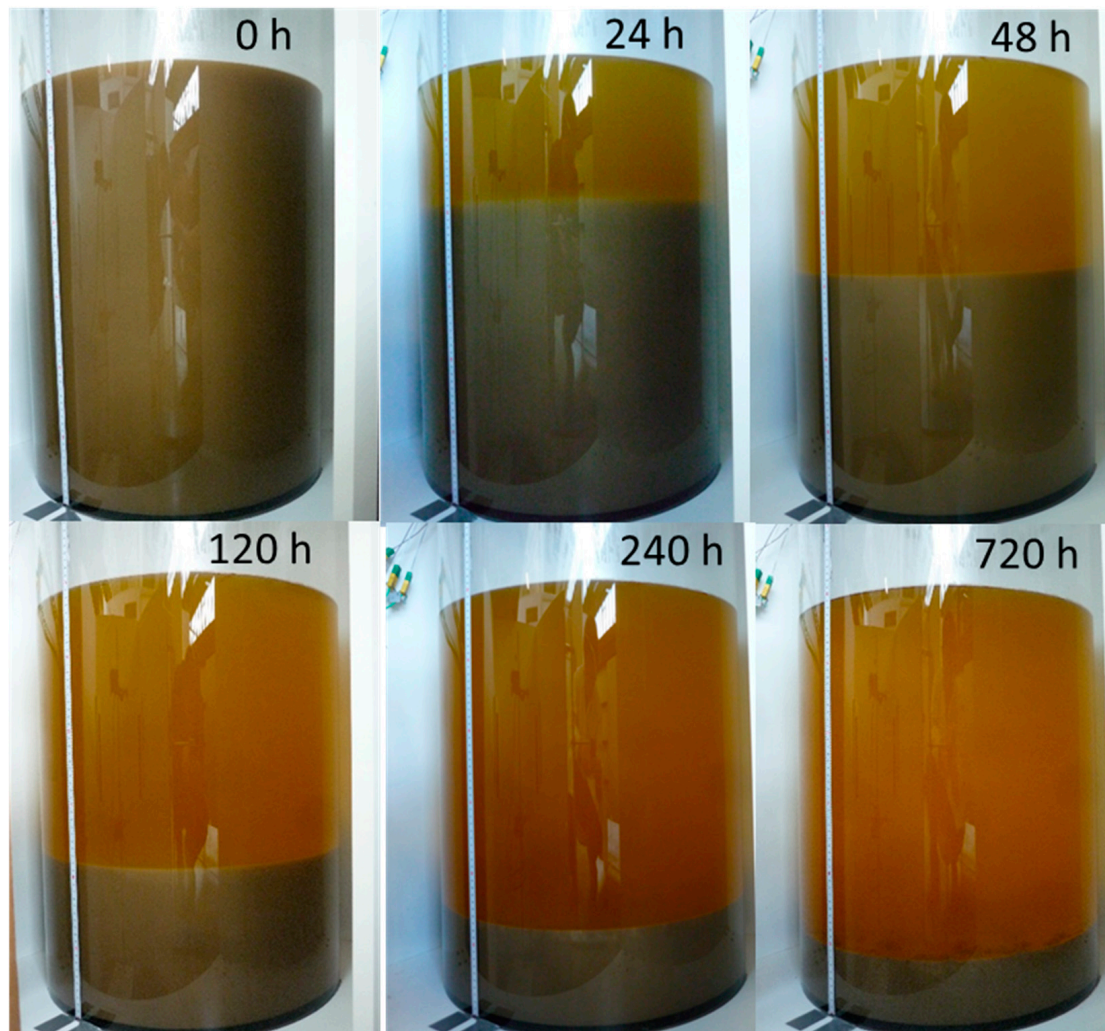


**Figure 4.** Images of the entire tank during the sedimentation process.

At 24 h, the interface was still blurred. This is likely because, as sedimentation continued, particles within the sample mainly settled individually at varying speeds due to differences in particle size or shape within the crude oil, resulting in a slightly spatial difference for the particles and a blurred interface. As the particles approached each other, their settling patterns became increasingly influenced by their proximity, leading them to settle more collectively as a whole. This resulted in a clearer interface and a sedimentation velocity smaller than  $-2$  mm/h at 48 h. As the sedimentation process persisted, the particles were increasingly compacted, thereby causing a continual decrease in the sedimentation velocity. According to the features of different sedimentation stages, we could confirm that at least diluted sedimentation and hindered sedimentation exist for the sesame oil sedimentation process.

The sedimentation velocity of diluted sedimentation is not related to the sedimentation tank's cross-section area. Karaj and Müller also found that both horizontal and vertical sedimentation system had the same sedimentation speed at the beginning of their sedimentation process [15]. Further, it is interesting that oil sedimentation velocity is at a magnitude millimeter per hour, while for wastewater it is millimeter per minute [39]—this could be

explained by the much higher viscosity of edible oil compared with water. In practice, when combining sedimentation with other oil-refining techniques, the rapid sedimentation velocity changing period could be a possible option to switch from sedimentation to other techniques. Additionally, for unrefined sesame oil producers (who typically only filter the oil after pressing), due to the nature of diluted sedimentation, it is possible for them to predict and control the time when an obvious sediment could be seen by customers.

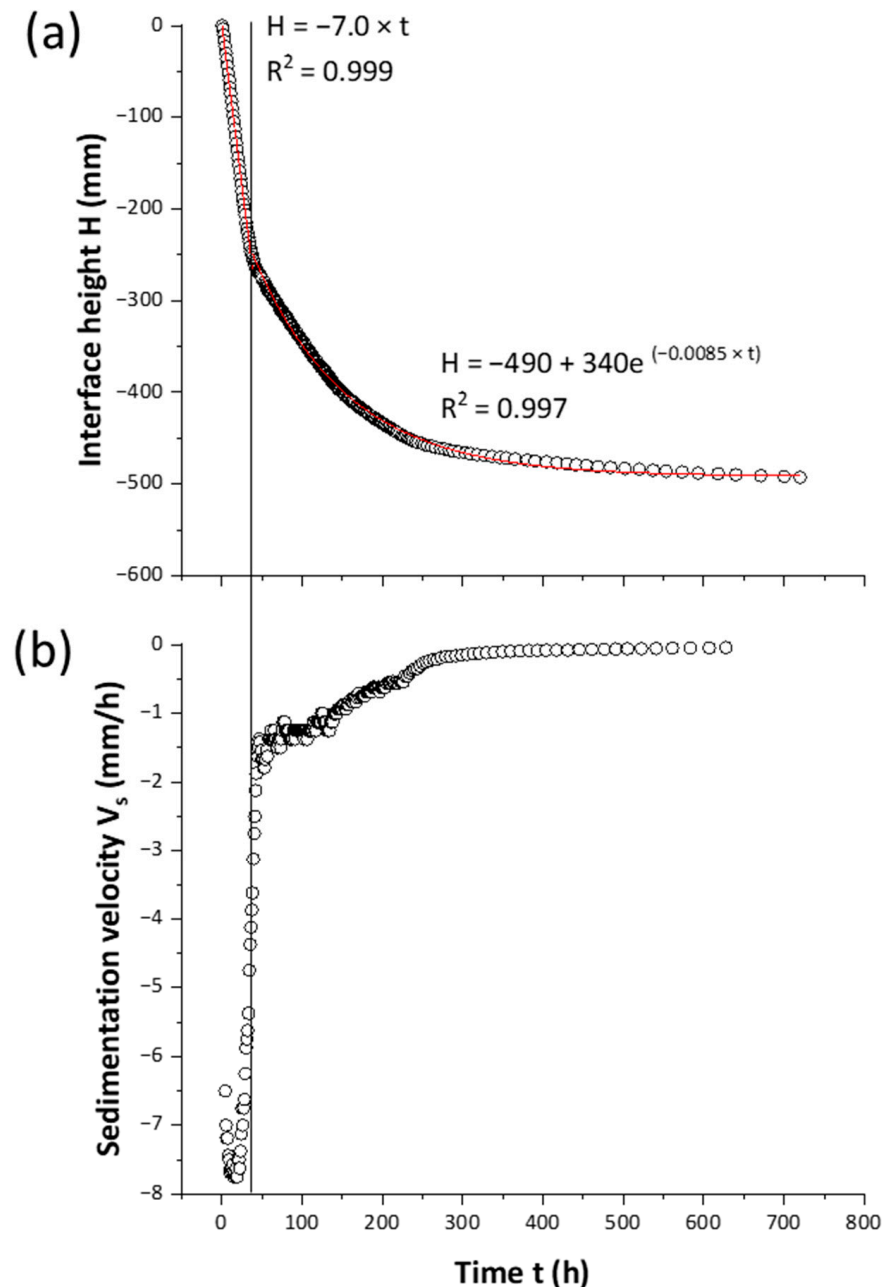


**Figure 5.** Plot of the (a) interface height vs. time and (b) the sedimentation velocity vs. time.

### 3.2.2. Backscattering Images

In Figure 6a, the temporal changes in backscattering images are illustrated. At the initial timepoint (0 h), the backscattering was characterized by a large scattering area with an overexposed center. As time progressed to 1 h, the scattering area notably reduced but the central region became even brighter. Subsequently, both the central brightness and the scattering area diminished, and at time 720 h, the overexposed center was no longer present. Figure 6b shows an “L” shape, where the backscattering shows a sharp change followed by

a gradual decrease over time. Notably, purplish hues were observed between the center and the surrounding scattering area, while in the discontinuous LBI measurement, it was yellow. Wu et al. indicated that this was caused by the different sensitivities of the camera color channels [37]. Additionally, the discontinuous LBI measurement showed the Tyndall effect (Figure 3) but it was not observed in Figure 6. This could be due to the lid on top of the sedimentation tank, which caused a reduction in laser light intensity when reaching the oil.

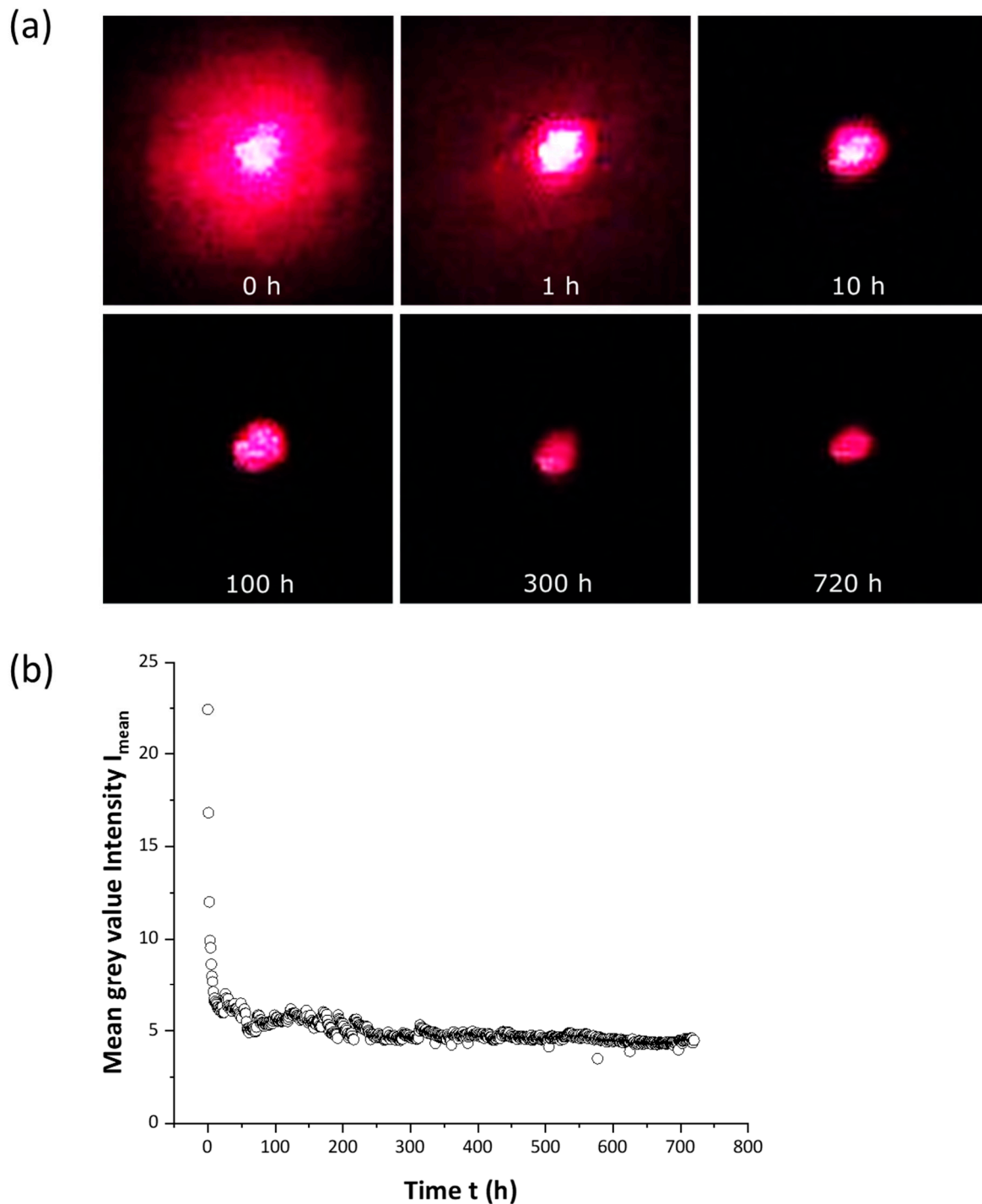


**Figure 6.** (a) Backscattering images during sedimentation in in situ experiment. (b) Plot of mean grey value of the segmented image vs. time.

### 3.2.3. Correlation between Backscattering Images and Oil Interface Height

Figure 7 illustrates the correlation between the height of the oil–sediment interface and the backscattering images. The scattering phenomenon decreased as the interface moved to a lower position, particularly when the interface height ranged between 0 and –100 mm. When the interface was lower, e.g., at –450 mm, a laser signal fluctuation could be observed. An exponential curve was initially used to fit this correlation, resulting in an  $R^2$  value of 0.73 (Figure 7a). As the sedimentation process progressed, the influence on the scattering spot located on the oil surface diminished, thereby increasing the difficulty of predicting the interface height based on the scattering spot. However, fitting the data with interface heights only between 0 and –100 mm using a power function resulted in an  $R^2$  of 0.97 (Figure 7b). This indicates that the scattering spots at the oil surface were more suitable for measuring the sedimentation process in the early stage of the diluted sedimentation. The Tyndall effect (Figure 3) may be more suitable for monitoring the entire sedimentation process. The laser’s traveling depth should be crucial for observation, indicating that decreasing the height of the sedimentation tank may not only speed up the sedimentation process [15] but also make laser scattering technology more suitable for monitoring the sedimentation process.

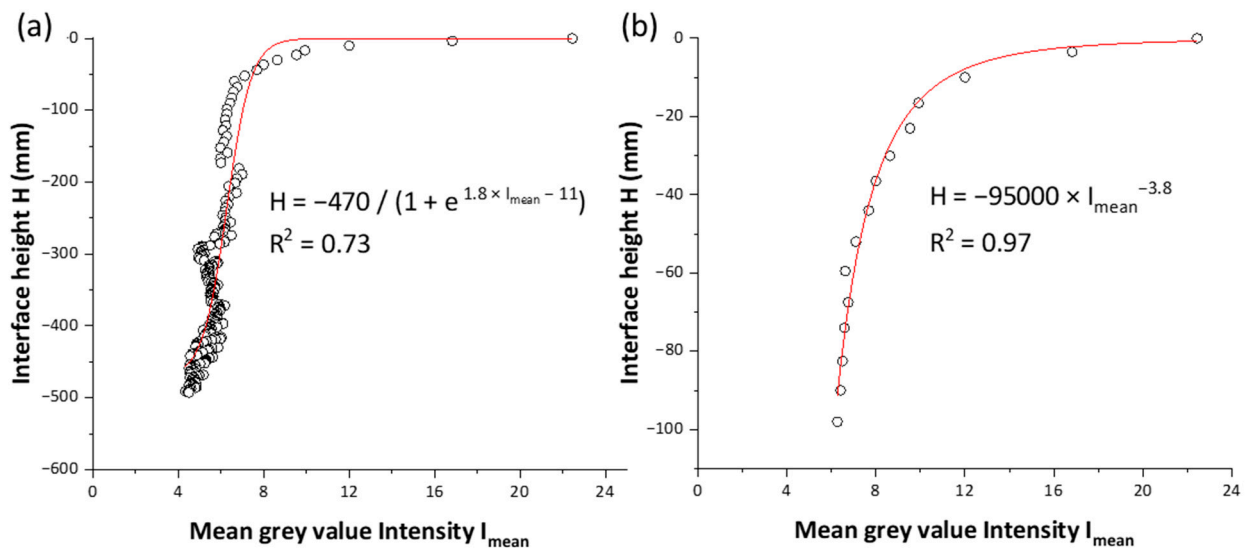


**Figure 7.** (a) Regression between interface height and mean grey value intensity  $I_{\text{mean}}$  of segmented images. (b) Regression when the interface height is less than 100 mm.

### 3.2.4. Chemical Properties

Table 2 presents the results of the comparison between the chemical properties before (Day 0) and after sedimentation (Day 30). Most of the parameters studied showed significant differences before and after sedimentation, with the exception of  $\delta$ -tocopherol and  $\gamma$ -tocopherol. Among all the changes in chemical properties, the ash content was not detectable after sedimentation. The total contamination decreased by 99.9% and the phosphorus content decreased by 99.5%, followed by water content (90%) and carbon residue (87%). The chemical properties that were strongly associated with the oil oxidation process—i.e., oxidation stability, vitamin E, and acid value—changed to a lesser degree. For pressed sesame oil, Mohammed et al. reported a phosphorus content of 1.14–3.94 mg/kg [40]; Melo et al. found an oxidation stability of 5.8 h and  $\gamma$ -tocopherol of 456  $\mu\text{g/g}$  [41]; Kheirati Rounizi et al. recorded an acid value of 3.68 mg/kg [42]. Differences between these values and those in our study may be attributed to variations in sesame seed quality or variety, extraction conditions, or storage methods.

**Table 2.** Chemical values of sesame oil measured before (Day 0) and after sedimentation (Day 30).

Parameter	Day 0	Day 30
Ash content (% <i>, m/m</i> )	0.84 <sup>a</sup> ± 0.02	0.00 <sup>b</sup> ± 0.00
Phosphorus content (mg/kg)	921 <sup>a</sup> ± 13	4.8 <sup>b</sup> ± 0.0
Carbon residue (% <i>, m/m</i> )	2.68 <sup>a</sup> ± 0.04	0.34 <sup>b</sup> ± 0.00
Total contamination (mg/kg)	48,170 <sup>a</sup> ± 1836	71 <sup>b</sup> ± 9
Water content (% <i>, m/m</i> )	0.86 <sup>a</sup> ± 0.02	0.09 <sup>b</sup> ± 0.00
Oxidation stability (h)	19.8 <sup>a</sup> ± 0.2	9.6 <sup>b</sup> ± 0.1
γ-Tocotrienol (μg/g)	1.106 <sup>a</sup> ± 0.108	0.858 <sup>b</sup> ± 0.088
δ-Tocopherol (μg/g)	5.200 <sup>a</sup> ± 0.512	4.717 <sup>a</sup> ± 0.272
γ-Tocopherol (μg/g)	333.32 <sup>a</sup> ± 26.07	314.80 <sup>a</sup> ± 12.59
Acid value (mg KOH/g)	0.98 <sup>a</sup> ± 0.02	1.82 <sup>b</sup> ± 0.03

Note: Values are means of replications ± standard deviation. Values in the same row with the same letter are not significantly different at  $p < 0.05$ .

Among all the measured chemical properties, ash content, phosphorus content, total contamination, and carbon residue should be mostly related to the particles present inside the crude oil. The settling of the particles caused more than an 86% drop in these values in the sesame oil. As for the 90% decrease in water content, Karaj and Müller related it to high-temperature evaporation [15]. Since the sesame oil was within  $21 \pm 3$  °C, it is more likely that the decrease in water content was also influenced by the consumption of H<sub>2</sub>O in the oil hydrolysis process. The decrease in oxidation stability and the increase in acid value are typical changes that occur during oil oxidation. However, the values of the two types of vitamin E (δ-tocopherol, γ-tocopherol) did not change significantly during the oxidation process. This could be because sesame oil contains additional antioxidants such as sesamin, sesamol, and sesamol, which protected vitamin E from decomposition [6]. After sedimentation, the measured chemical values did not meet the requirements of combustion engines (total contamination upper limitation, 24 mg/kg) [43] but were suitable for food (acid value) [44] and pressure stoves (acid value and total contamination) [14,45].

#### 4. Conclusions

In the application of LBI to the sedimentation process of sesame oil, two types of scattering effects were observed. The first was a typical scattering spot at the oil's surface, and the second was a Tyndall effect with an increasingly extended path as the sedimentation process continued. The scattering spot at the surface of the oil should be more suitable for monitoring the early stage of diluted sedimentation while the Tyndall effect should be better suited for monitoring the entire process. The crude sesame oil sedimentation process consists of at least two stages: diluted sedimentation and hindered sedimentation. In this study, the sedimentation speed was about  $-7$  mm/h during the diluted sedimentation stage and then dropped to less than  $-2$  mm/h, indicating the transition into the hindered sedimentation stage. During the sedimentation process, three factors influenced the oil properties: settling of the particles, oxidation, and hydrolysis. The low change in vitamin E content may be due to the antioxidants of the sesame oil.

It is implied that when the volume of a sedimentation tank is fixed, increasing the cross-section and decreasing the height can speed up the sedimentation process and benefit the application of low-cost laser backscattering technology. For producers who make unrefined sesame oil, confirming the diluted sedimentation stage can help them control the time when the customer will see the sedimentation. The laser's power was 1 mW in the continuous LBI measurement. Further research could use a higher-power laser source to enhance both the scattering on the oil surface and the Tyndall effects inside the oil. Additionally, experiments with more plant oil varieties could be conducted to extend the applicability of the LBI technology. It is worth noting that the sedimentation tank design method was greatly improved in the field of wastewater treatment. People interested in plant oil sedimentation may benefit from the similarity between these two processes.

**Author Contributions:** Conceptualization, Z.W. and S.R.; methodology, Z.W., S.R. and K.I.; software, Z.W.; validation, Z.W.; formal analysis, Z.W.; investigation, Z.W.; resources, Z.W. and S.R.; data curation, Z.W.; writing—original draft preparation, Z.W.; writing—review and editing, Z.W., S.R., K.I. and J.M.; visualization, Z.W. and S.R.; supervision, S.R. and J.M.; project administration, S.R.; funding acquisition, S.R. and J.M. All authors have read and agreed to the published version of the manuscript.

**Funding:** This work was funded by Bundesministerium für wirtschaftliche Zusammenarbeit und Entwicklung (BMZ), grant number PN 13.6254.0-004.0, under the project “Performance optimization of a solar oil press for the productive extraction of sesame oil in Burkina Faso”, in the framework of Deutsche Gesellschaft für Internationale Zusammenarbeit (GIZ) Powering Agriculture. This work was also funded by China Scholarship Council, grant number No. 201406350068.

**Institutional Review Board Statement:** Not applicable.

**Informed Consent Statement:** Not applicable.

**Data Availability Statement:** Not applicable.

**Acknowledgments:** Special thanks to Tsubasa Mitsui, Ute Waldeck, Olga Gotra, Sarah Fleischmann, and Nadine Grebenstein for their assistance in conducting the experiment.

**Conflicts of Interest:** The authors declare no conflict of interest.

## References

1. FAO, Food and Agriculture Organization of the United Nations. Available online: <https://www.fao.org/faostat/en/#data/QCL> (accessed on 6 March 2023).
2. Rezaei, M.; Ramezani, M. Physicochemical Properties of Heavy Metals and Aflatoxin Levels in Sesame Oil: A Review Study. *J. Nutr. Fasting Health* **2018**, *6*, 45–51. [[CrossRef](#)]
3. Sallam, K.I.; Abd-Elghany, S.M.; Imre, K.; Morar, A.; Herman, V.; Hussein, M.A.; Mahros, M.A. Ensuring Safety and Improving Keeping Quality of Meatballs by Addition of Sesame Oil and Sesamol as Natural Antimicrobial and Antioxidant Agents. *Food Microbiol.* **2021**, *99*, 103834. [[CrossRef](#)] [[PubMed](#)]
4. Alshahrani, S.; Al Sreaya, A.A.; Mashyakh, M.Y.; Alqahtani, S.; Sivakumar, S.M.; Alhazmi, H.A.; Rehman, Z.; Alam, F. Chemical Characterization and Antibacterial Efficacy of Saudi Sesame Oil against Human Pathogenic Bacteria. *Environ. Conserv. J.* **2020**, *21*, 19–29. [[CrossRef](#)]
5. Langyan, S.; Yadava, P.; Sharma, S.; Gupta, N.C.; Bansal, R.; Yadav, R.; Kalia, S.; Kumar, A. Food and Nutraceutical Functions of Sesame Oil: An Underutilized Crop for Nutritional and Health Benefits. *Food Chem.* **2022**, *389*, 132990. [[CrossRef](#)] [[PubMed](#)]
6. Mujtaba, M.A.; Muk Cho, H.; Masjuki, H.H.; Kalam, M.A.; Ong, H.C.; Gul, M.; Harith, M.H.; Yusoff, M.N.A.M. Critical Review on Sesame Seed Oil and Its Methyl Ester on Cold Flow and Oxidation Stability. *Energy Reports* **2020**, *6*, 40–54. [[CrossRef](#)]
7. Soltani, H.; Karimi, A.; Falahatpisheh, S. The Optimization of Biodiesel Production from Transesterification of Sesame Oil via Applying Ultrasound-Assisted Techniques: Comparison of RSM and ANN-PSO Hybrid Model. *Chem. Prod. Process Model.* **2022**, *17*, 55–67. [[CrossRef](#)]
8. Mahlouljifar, M.; Mansournia, M. A Comparative Study on the Catalytic Performances of Alkali Metals-Loaded KAISiO<sub>4</sub> for Biodiesel Production from Sesame Oil. *Fuel* **2021**, *291*, 120145. [[CrossRef](#)]
9. Ahmad, R. Gravity Separation/Sedimentation. In *Water Encyclopedia*; Wiley: Hoboken, NJ, USA, 2005; pp. 259–261. ISBN 9780471478447.
10. Vaisali, C.; Charanyaa, S.; Belur, P.D.; Regupathi, I. Refining of Edible Oils: A Critical Appraisal of Current and Potential Technologies. *Int. J. Food Sci. Technol.* **2015**, *50*, 13–23. [[CrossRef](#)]
11. Santori, G.; Di Nicola, G.; Moglie, M.; Polonara, F. A Review Analyzing the Industrial Biodiesel Production Practice Starting from Vegetable Oil Refining. *Appl. Energy* **2012**, *92*, 109–132. [[CrossRef](#)]
12. Gupta, M.K. Refining. In *Practical Guide to Vegetable Oil Processing*; Elsevier: Amsterdam, The Netherlands, 2017; pp. 79–128. ISBN 9781630670504.
13. Altieri, G.; Di Renzo, G.C.; Genovese, F.; Tauriello, A.; D’Auria, M.; Racioppi, R.; Viggiani, L. Olive Oil Quality Improvement Using a Natural Sedimentation Plant at Industrial Scale. *Biosyst. Eng.* **2014**, *122*, 99–114. [[CrossRef](#)]
14. Karaj, S.; Müller, J. Influence of Total Contamination of *Jatropha Curcas* Oil on Deposits and Performance of Plant Oil Pressure Stoves. In Proceedings of the European Biomass Conference and Exhibition Proceedings, Milan, Italy, 18–22 June 2012; pp. 1311–1315.
15. Karaj, S.; Müller, J. Effect of Container Depth and Sedimentation Time on Quality of *Jatropha curcas* L. Oil. *Fuel* **2014**, *118*, 206–213. [[CrossRef](#)]

16. Davis, J.P.; Geller, D.; Faircloth, W.H.; Sanders, T.H. Comparisons of Biodiesel Produced from Unrefined Oils of Different Peanut Cultivars. *JAOCs, J. Am. Oil Chem. Soc.* **2009**, *86*, 353–361. [[CrossRef](#)]
17. Hiron, K.; Devi, T.T. Application of Computational Fluid Dynamics in Sedimentation Tank Design and Its Recent Developments: A Review. *Water, Air, Soil Pollut.* **2022**, *233*, 22. [[CrossRef](#)]
18. Oleador GmbH. Available online: <https://www.oleador.com/en/contact/faq-detail-Oils,deposit-66.html> (accessed on 10 March 2023).
19. Rushton, A.; Ward, A.S.; Holdich, R.G. Sedimentation Fundamentals. In *Solid-Liquid Filtration and Separation Technology*; Wiley-VCH: Weinheim, Germany, 1996. Available online: <https://download.e-bookshelf.de/download/0000/6032/15/L-G-0000603215-0002288622.pdf> (accessed on 10 March 2023).
20. Pietsch, T.; Mehrwald, R.; Grajetzki, R.; Sens, J.; Märkl, H. Sedimentation Behaviour of Sludge Particles in a Biogas Tower Reactor and the Function of a Hydrostatically Pressurized Sedimenter. *Water Res.* **2003**, *37*, 1071–1079. [[CrossRef](#)]
21. Mollazade, K.; Omid, M.; Tab, F.A.; Mohtasebi, S.S. Principles and Applications of Light Backscattering Imaging in Quality Evaluation of Agro-Food Products: A Review. *Food Bioprocess Technol.* **2012**, *5*, 1465–1485. [[CrossRef](#)]
22. Lu, B.; Dao, P.D.; Liu, J.; He, Y.; Shang, J. Recent Advances of Hyperspectral Imaging Technology and Applications in Agriculture. *Remote Sens.* **2020**, *12*, 2659. [[CrossRef](#)]
23. Sanchez, P.D.C.; Hashim, N.; Shamsudin, R.; Mohd Nor, M.Z. Potential Application of Laser-Based Imaging Technology in the Quality Evaluation of Agricultural Products: A Review. *Adv. Agric. Food Res. J.* **2020**, *1*, 243–256. [[CrossRef](#)]
24. Kiliçkan, A.; Üçer, N.; Yalçın, I. Moisture-Dependent Physical Properties of Grape (*Vitis vinifera* L.) Seed. *Sci. Res. Essays* **2010**, *5*, 2226–2233.
25. *ISO 6884*; Animal and Vegetable Fats and Oils—Determination of Ash. ISO: Geneva, Switzerland, 1985.
26. *DIN EN ISO 11885*; Water Quality—Determination of Selected Elements by Inductively Coupled Plasma Optical Emission Spectrometry (ICP-OES) (ISO 11885:2007). Beuth: Berlin, Germany, 2009. [[CrossRef](#)]
27. *DIN EN 14107*; Fat and Oil Derivatives—Fatty Acid Methyl Esters (FAME)—Determination of Phosphorus Content by Inductively Coupled Plasma (ICP) Emission Spectrometry. Beuth: Berlin, Germany, 2003. [[CrossRef](#)]
28. *DIN EN ISO 10370*; Petroleum Products—Determination of Carbon Residue—Micro Method (ISO 10370:1993). Beuth: Berlin, Germany, 1995.
29. *DIN EN 12662*; Liquid Petroleum Products—Determination of Contamination in Middle Distillate. Beuth: Berlin, Germany, 2008.
30. *DIN EN ISO 12937*; Petroleum Products—Determination of Water—Coulometric Karl Fischer Titration Method (ISO 12937:2000). Beuth: Berlin, Germany, 2002. [[CrossRef](#)]
31. *DIN EN 14112*; Fat and Oil Derivatives—Fatty Acid Methyl Esters (FAME)—Determination of Oxidation Stability (Accelerated Oxidation Test). Beuth: Berlin, Germany, 2016. [[CrossRef](#)]
32. Grebenstein, N.; Frank, J. Rapid Baseline-Separation of All Eight Tocopherols and Tocotrienols by Reversed-Phase Liquid-Chromatography with a Solid-Core Pentafluorophenyl Column and Their Sensitive Quantification in Plasma and Liver. *J. Chromatogr. A* **2012**, *1243*, 39–46. [[CrossRef](#)]
33. SI Analytics. Determination of Acid Number and Free Fatty Acids (FFA) in Fats and Oils. (DGF-Einheitsmethoden C-V 2). Available online: [https://uk.vwr.com/m-uk.vwr.com/en\\_GB/images/Acidity-in-fats-and-oils-FFA\\_285KB\\_English-PDF.pdf](https://uk.vwr.com/m-uk.vwr.com/en_GB/images/Acidity-in-fats-and-oils-FFA_285KB_English-PDF.pdf) (accessed on 6 April 2023).
34. Lorente, D.; Zude, M.; Idler, C.; Gómez-Sanchis, J.; Blasco, J. Laser-Light Backscattering Imaging for Early Decay Detection in Citrus Fruit Using Both a Statistical and a Physical Model. *J. Food Eng.* **2015**, *154*, 76–85. [[CrossRef](#)]
35. Adebayo, S.E.; Hashim, N.; Abdan, K.; Hanafi, M. Application and Potential of Backscattering Imaging Techniques in Agricultural and Food Processing—A Review. *J. Food Eng.* **2016**, *169*, 155–164. [[CrossRef](#)]
36. Sanchez, P.D.C.; Hashim, N.; Shamsudin, R.; Mohd Nor, M.Z. Quality Evaluation of Sweet Potatoes (*Ipomoea batatas* L.) of Different Varieties Using Laser Light Backscattering Imaging Technique. *Sci. Hortic.* **2020**, *260*, 108861. [[CrossRef](#)]
37. Wu, Z.; Spohrer, K.; Nagle, M.; Müller, J. Investigating the Influence of Pore Size, Pore Fluid and Wavelength on Backscattering Images with Sintered Glass Filter Matrices as Experimental Models. *Postharvest Biol. Technol.* **2023**, *200*, 112329. [[CrossRef](#)]
38. Huang, J.; Mo, X.; Fu, H.; Sun, Y.; Gao, Q.; Chen, X.; Zou, J.; Yuan, Y.; Nie, J.; Zhang, Y. Tyndall-Effect-Enhanced Supersensitive Naked-Eye Determination of Mercury (II) Ions with Silver Nanoparticles. *Sensors Actuators, B Chem.* **2021**, *344*, 130218. [[CrossRef](#)]
39. Song, Z.; Williams, C.J.; Edyvean, R.G.J. Sedimentation of Tannery Wastewater. *Water Res.* **2000**, *34*, 2171–2176. [[CrossRef](#)]
40. Mohammed, F.; Abdulwali, N.; Guillaume, D.; Tenyang, N.; Ponka, R.; Al-Gadabi, K.; Bchitou, R.; Abdullah, A.H.; Naji, K.M. Chemical Composition and Mineralogical Residence of Sesame Oil from Plants Grown in Different Yemeni Environments. *Microchem. J.* **2018**, *140*, 269–277. [[CrossRef](#)]
41. Melo, D.; Álvarez-ortí, M.; Nunes, M.A.; Costa, A.S.G.; Machado, S.; Alves, R.C.; Pardo, J.E.; Oliveira, M.B.P.P. Whole or Defatted Sesame Seeds (*Sesamum indicum* L.)? The Effect of Cold Pressing on Oil and Cake Quality. *Foods* **2021**, *10*, 2108. [[CrossRef](#)] [[PubMed](#)]
42. Kheirati Rounizi, S.; Akrami Mohajeri, F.; Moshtaghi Broujeni, H.; Pourramezani, F.; Jambarsang, S.; Kiani, H.; Khalili Sadrabad, E. The Chemical Composition and Heavy Metal Content of Sesame Oil Produced by Different Methods: A Risk Assessment Study. *Food Sci. Nutr.* **2021**, *9*, 2886–2893. [[CrossRef](#)]
43. *DIN 51623*; Fuels for Vegetable Oil Compatible Combustion Engines—Fuel from Vegetable Oil—Requirements and Test Methods. Beuth: Berlin, Germany, 2020. [[CrossRef](#)]

44. CXS 210-1999; Standard for Named Vegetable Oils. FAO: Rome, Italy, 2022. Available online: <https://www.fao.org/fao-who-codexalimentarius/codex-texts/list-standards/en/> (accessed on 6 March 2023).
45. Kratzeisen, M.; Müller, J. Influence of Free Fatty Acid Content of Coconut Oil on Deposit and Performance of Plant Oil Pressure Stoves. *Fuel* **2010**, *89*, 1583–1589. [[CrossRef](#)]

**Disclaimer/Publisher’s Note:** The statements, opinions and data contained in all publications are solely those of the individual author(s) and contributor(s) and not of MDPI and/or the editor(s). MDPI and/or the editor(s) disclaim responsibility for any injury to people or property resulting from any ideas, methods, instructions or products referred to in the content.